J Membrane Biol (2014) 247:319–330
DOI 10.1007/s00232-014-9634-3

Shaker IR T449 Mutants Separate C- from U-Type Inactivation

Quentin Jamieson · Stephen W. Jones

Received: 4 November 2013 / Accepted: 13 January 2014 / Published online: 1 February 2014

Abstract Previous studies demonstrated that slow inactivation of the Shaker potassium channel can be made ~100-fold faster or slower by point mutations at a site in the outer pore (T449). However, the discovery that two forms of slow inactivation coexist in Shaker raises the question of which inactivation process is affected by mutation. Equivalent mutations in $K_V2.1$, a channel exhibiting only U-type inactivation, have minimal effects on inactivation, suggesting that mutation of Shaker T449 acts on C-type inactivation alone, a widely held yet untested hypothesis. This study reexamines mutations at Shaker T449, confirming that T449A speeds inactivation and T449Y/V slow it. T449Y and T449V exhibit U-type inactivation that is enhanced by high extracellular potassium, in contrast to C-type inactivation in T449A which is inhibited by high potassium. Automated parameter estimation for a 12-state Markov model suggests that U-type inactivation occurs mainly from closed states upon weak depolarization, but primarily from the open state at positive voltages. The model also suggests that WT channels, which in this study exhibit mostly C-type inactivation, recover from inactivation through closed-inactivated states, producing voltage-dependent recovery. This suggests that both C-type and U-type inactivation involve both open-inactivated and closed-inactivated states.

Keywords C-type inactivation · U-type inactivation · Voltage-dependent potassium channels · Kinetic models

Introduction

N-terminally truncated Shaker channels with "inactivation removed" (Shaker IR) exhibit a slow inactivation mechanism (Hoshi et al. 1991) which is dramatically affected by mutations at outer-pore residue T449 (López-Barneo et al. 1993). Mutations of T449 can slow or speed inactivation up to 100-fold, and this "hot spot" of inactivation has been canonically ascribed to affect C-type inactivation. However, since characterization of the T449 mutations, U-type inactivation has been discovered to coexist with C-type inactivation in Shaker IR (Klemic et al. 2001) raising questions as to whether mutations of Shaker T449 affect C-type inactivation, U-type inactivation, or both.

The molecular mechanism underlying C-type inactivation is now well understood and the originally proposed pore collapse mechanism (Ogielska et al. 1995; Liu et al. 1996) has been described in greater molecular detail (Cordero-Morales et al. 2007, 2006; Cuello et al. 2010). However, the molecular determinants of U-type inactivation remain largely unknown. Mutational analysis in both $K_V2.1$ and $K_V4.2$ channels suggests that sites near the S4 voltage-sensing domain and S6 activation gate are potential candidates underlying U-type inactivation (Kerschensteiner et al. 2003; Dougherty et al. 2008; Barghaan and Bähring 2009). For $K_V2.1$, the near-pore region may be involved (Cheng et al. 2011), but mutation of Y380 (the equivalent site to Shaker T449) had little effect (Jamieson and Jones 2013). These mixed results motivated a more in-depth examination of which inactivation mechanism is affected by mutations of Shaker T449.

Electronic supplementary material The online version of this article (doi:10.1007/s00232-014-9634-3) contains supplementary material, which is available to authorized users.

Q. Jamieson · S. W. Jones (✉)
Department of Physiology and Biophysics, Case Western Reserve University, Cleveland, OH 44106, USA
e-mail: swj@case.edu

C-type and U-type inactivation have distinct kinetic and pharmacological properties, which should enable an analysis of how a mutation affects each mechanism. For example, recovery from inactivation in Shaker IR is dramatically biexponential (Klemic et al. 2001) having fast and strongly voltage-dependent recovery from U-type inactivation yet slow and weakly voltage-dependent recovery from C-type inactivation. Additionally, C-type inactivation is inhibited by extracellular application of the large organic cation TEA^+ (Choi et al. 1991) or elevated K^+ (López-Barneo et al. 1993; Baukrowitz and Yellen 1996), whereas elevated K^+ accelerates U-type inactivation (Klemic et al. 1998). How a mutation influences each of these phenomena can discriminate which inactivation mechanism is affected.

This study examined wild-type (WT) Shaker IR channels and a subset of mutants from the study by López-Barneo et al., including mutations which either slowed or accelerated inactivation. Should mutants selectively affect C-type inactivation, those which accelerate inactivation should exhibit chiefly C-type inactivation, whereas those which decelerate it should demonstrate weak (if any) C-type inactivation. Surprisingly, WT channels lacked U-type inactivation, in contrast to the previous report (Klemic et al. 2001) on Shaker IR in Xenopus oocytes. The T449A mutant, which hastens inactivation, had C-type inactivation characteristics, whereas the T449Y and T449V mutants, which slow inactivation, exhibited features of U-type inactivation. Model simulations suggest that both mechanisms may reflect a mix of both open- and closed-state inactivation.

Materials & Methods

Cell Culture & Electrophysiology

Shaker IR, derived from Shaker H4 with N-terminal residues Δ6–46 removed, including mutations C301S, C308S, and T449V, and contained within the GW1-CMV expression vector was a generous gift of Dr. Gary Yellen. Molecular biology, cell culture, and electrophysiological techniques were as described previously (Jamieson and Jones 2013). Briefly, Shaker IR was subcloned into a tetracycline-inducible expression system using T-REx-293 cells (Invitrogen, Grand Island, NY) to control channel expression in a time- and concentration-dependent manner (Trapani and Korn 2003), because high expression levels tended to produce excessively large currents with the GW1-CMV vector. Mutations were generated at outer-pore residue 449 to generate 4 constructs: WT, T449A, T449V, and T449Y channels. Stably transfected polyclonal cell lines were established for both WT and mutant channels using antibiotic selection. Before performing whole-cell patch-clamp experiments, cells were incubated with tetracycline for 3–5 h (in μg/mL, WT: 15, T449A: 20, T449Y: 20, and T449V: 10) to induce expression. Data were recorded at room temperature using an Axopatch 200 amplifier (Axon Instruments). Cells were chosen which expressed currents between 4 and 20 nA at +60 mV to minimize series resistance error, or ion depletion effects (Frazier et al. 2000). The whole-cell capacitance was 9.6 ± 2.9 pF and series resistance was 2.1 ± 0.7 MΩ ($n = 117$, values ± standard deviation) before being compensated at 80–90 %.

A three-pulse protocol was used to measure the time and voltage dependence of inactivation with strong depolarization (−20 to +60 mV, or −40 to +60 for T449A) (e.g., Fig. 2). The length of the inactivating pulse was chosen to inactivate a significant fraction, but not all, of the channels. Measuring inactivation prior to steady state is a more sensitive test for a U-shaped voltage dependence, as noted previously for Shab (Drosophila K_V2) (Carrillo et al. 2013). The extent of inactivation is thus affected by both the rate and steady-state level of inactivation.

The kinetics of inactivation were evaluated by fitting currents during the three-pulse protocol to the sum of two exponential components. This provided a more accurate fit to the time course of inactivation than a single exponent, except for the rapidly inactivating T449A mutant, where fits to a single exponential were adequate. We do not interpret these components as representing separate inactivation processes (e.g., C- and U-type inactivation) as discussed previously (Klemic et al. 2001). The fits yielded a sizable non-inactivating component in all channels studied, smallest in T449A (~10 %) and largest with T449Y or T449V (~30 %).

Recording Solutions

The intracellular pipette and extracellular bath solutions were prepared, buffered, and titrated to pH 7.2 as previously described (Jamieson and Jones 2013). The intracellular solution contained (in mM): 120 KCl, 2 CaCl2, 1 MgCl2, 11 EGTA, 10 HEPES, and 4 MgATP. The extracellular bath contained (in mM): 135 NaCl, 5 KCl, 2 CaCl2, 10 HEPES, and 10 glucose. In experiments studying blockade by extracellular TEA^+, NaCl was replaced by equimolar substitution with TEA-Cl. A concentration of TEA-Cl was used that half-maximally blocked channels (20 mM TEA^+ blocked WT channels 46.0 ± 1.5 %, 30 mM blocked T449A 47.1 ± 1.8 %, 1 mM blocked T449Y 50.8 ± 0.7 %, and 50 mM blocked T449V 43.5 ± 1.8 %). For studies examining the effect of elevated extracellular potassium, bath KCl was increased to 60 mM by equimolar substitution with NaCl.

Model Simulation

The 12-state Markov model for inactivation of $K_V2.1$ channels was adapted for use with Shaker IR and simulated in MATLAB Version R2012b (The MathWorks, Inc) using the Q-matrix method (Colquhoun and Hawkes 1995) as previously described (Jamieson and Jones 2013). Briefly, model parameters were determined using constrained nonlinear optimization, minimizing the difference between experimental current traces and simulated open probabilities, converted to current with a driving force correction. Although the current traces were fitted directly (data point by data point), we also compare results of exponential fitting of experimental data to the model for qualitative visual evaluation of the quality of the fit. The global optimization algorithm "MultiStart" was used to find the minimum fitting error within a specified subset of parameter space for each dataset. A detailed description of simulation methods is supplied in supplementary material. All computational work were performed with laboratory computers and the CWRU ITS High Performance Computing Cluster using the MATLAB Distributed Computing Engine.

Statistics

All data values are presented as mean ± SE except where otherwise noted. A paired Student's *t* test was used to evaluate statistical differences between mutant and WT channels. A two-tailed p value of 0.05 was used to determine statistical significance. In most cases, statistical significance was evaluated using fitted curves except where noted when significance was evaluated for individual voltages or pharmacological conditions.

Electronic Supplementary Material

Fig. S1 compares resultant currents from different measurements of channel activation (IIV versus IV) for different mutants. Fig. S2 compares the time course of inactivation for different mutants with superimposed biexponential fits. Fig. S3 compares inactivation with weak depolarization among different mutants. Fig. S4 compares the time course of recovery from inactivation at −90 mV between different mutants. Fig. S5 compares recovery from inactivation at a given voltage for different mutants. Fig. S6 compares the kinetic scheme of the Klemic et al. (1998) allosteric model for inactivation of $K_V2.1$ with a simplified model permitting only open-state inactivation. Figs. S7–S14 compare the best 8 model simulations of voltage-dependent phenomena superimposed on data for each of the channel mutants. Fig. S15 compares the simulated and experimental time course of inactivation among different datasets. Fig. S16 compares the simulated and experimental time course of recovery from inactivation for different datasets. Tables S1–S3 summarize the experimental measurements of activation and inactivation kinetics. Table S4 shows the best-fit model parameter sets for each experimental dataset. Table S5 shows the 8 best-fit model parameter sets for T449V dataset V2. The Supplementary Text includes additional information on parameter estimation.

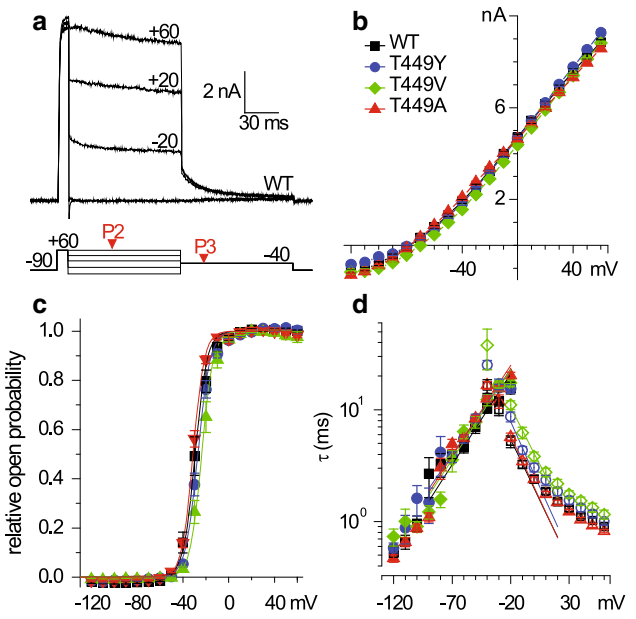

Fig. 1 Activation: **a** IIV protocol, WT currents in response to depolarization to +60 mV for 10 ms, repolarized (P2) from −120 mV to +60 mV for 100 ms (shown here −120, −70, −20, +20, +60 mV), and finally to −40 mV (P3) for 100 ms. Cell D110127. **b** Peak tail currents in Fig. 1a during P2 are plotted versus voltage to produce the IIV curve for WT (*squares*), T449Y (*circles*), T449V (*diamonds*), and T449A (*triangles*) channels. Identifying symbols used throughout manuscript. T449V is statistically different from WT in the range [−80, −50] mV. **c** Peak tail currents from the IIV protocol during P3 (or in Fig. S1b, P2 from the IV protocol) are normalized to peak tail current at +60 mV and plotted versus depolarizing voltage (from −120 to +60 mV) to depict the voltage dependence of channel activation. *This figure* represents the average of activation curves from the IIV and IV protocols. *Symbols* correspond to mutants as in Fig. 1b. *Solid lines* represent fits to a first-order Boltzmann function. **d** Time constants from monoexponential fits to channel deactivation (Fig. 1a, IIV protocol, P2) are shown as *solid symbols* from −120 to −20 mV. Time constants from similar fits to channel activation (Fig. S1b, IV protocol, P1) are shown as open symbols from −40 to +60 mV. *Lines* represent logarithmic fits to time constants. T449Y is statistically different from WT in the range [−30, 0] mV, T449V in the range [−30, 50] mV. WT ($n = 10$), T449A ($n = 13$), T449Y ($n = 10$), T449V ($n = 11$)

Results

T449 Mutants Have Little Effect on Shaker Activation

Controlling for possible effects of mutations on activation is critical, since both C-type and U-type inactivation are thought to be coupled to the channel activation process. If a mutation did affect activation, understanding how that mutation affects the inactivation mechanism requires accounting to the effects on the activation mechanism. A strong effect on activation could even question whether Shaker T449 has any direct effect on the inactivation process.

Two standard protocols were used to characterize the kinetics of activation and deactivation over a wide voltage range. The instantaneous current–voltage protocol (IIV) first preactivates the channels by a brief strong depolarization, and then examines tail currents over a wide range of voltages (Fig. 1a). In response to the IIV protocol, WT Shaker channels activate rapidly with a time constant of 0.90 ± 0.05 ms ($n = 10$) at +60 mV, before deactivating upon repolarization. The decay in current seen during P2 at more positive voltages is due to slow inactivation. The resulting instantaneous I–V curve (Fig. 1b) demonstrates a non-linear voltage dependence of permeation for both WT and mutant channels.

Activation was also characterized with the IV protocol, similar to the protocol of Fig. 1a but without the pre-pulse to +60 mV. The resultant currents from this protocol are seen in Fig. S1b in the supplementary material. Representative currents from the IIV and IV protocols are shown for each of the three mutants (labeled separately in Fig. S1).

In Fig. 1c, the voltage dependence of activation is shown as the average of the activation curves determined from the IIV and IV protocols (activation curves shown separately in Fig. S1). A first-order Boltzmann function was fit to each mutant's activation curve finding that none was statistically different from WT channels. For example, T449A channels are half maximally activated at −31.2 ± 0.7 mV ($n = 13$) versus WT channels at −29.3 ± 1.9 mV ($n = 10$). Furthermore, both the IIV and IV protocols produced similar measures of channel activation. For T449A, where the difference was the largest, half-maximal activation was at −32.3 ± 0.8 mV (IIV) versus −30.1 ± 0.7 mV (IV). Table S1 compares all mutants.

Time constants from a monoexponential fit to the rising (activating) phase of the IV protocol (Fig. S1b, P1) and the decaying (deactivating) phase of the IIV protocol (Fig. 1a, P2) were measured at each voltage step tested and for each mutant (Fig. 1d). Although no mutant had deactivation kinetics statistically different from WT channels, both T449Y and T449V activated more slowly than WT channels, e.g., at −30 mV, WT channels activated with a time constant of 10.0 ± 1.2 ms versus 16.9 ± 1.2 ms for T449V.

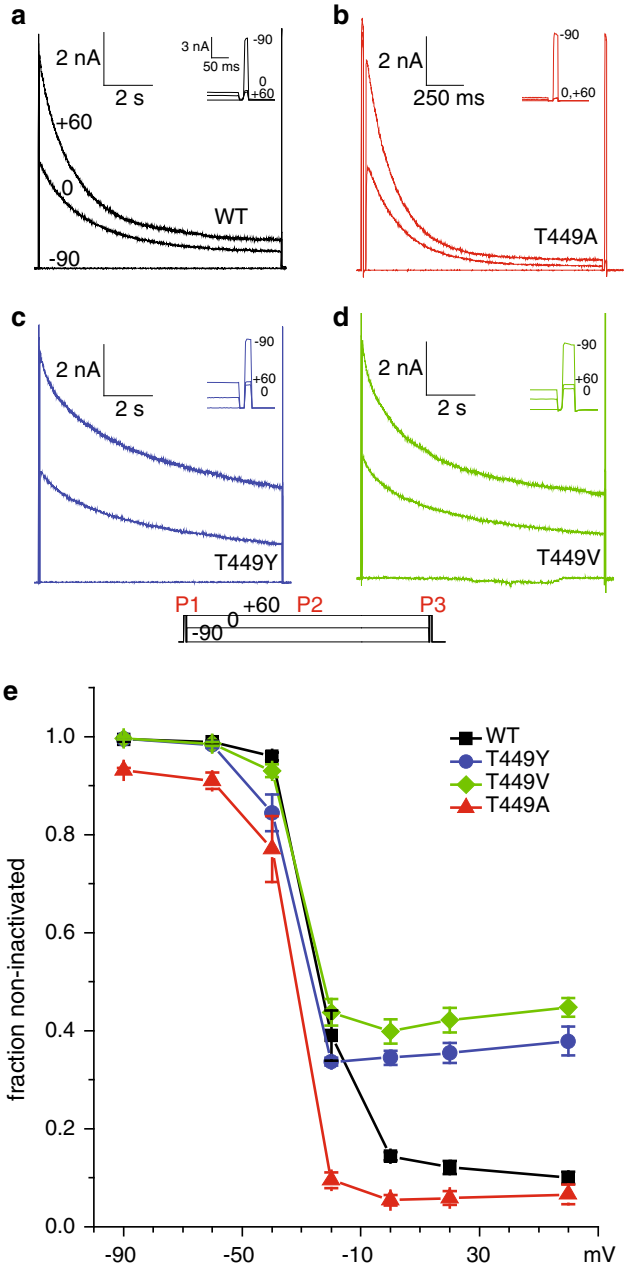

Fig. 2 Inactivation: 20 ms test pulses measure the amplitude of non-inactivated channels before (P1) and after (P3) a 10-second inactivating pulse from −90 to +60 mV in 10 mV increments (shown here −90, 0, and +60 mV) for **a** WT (cell A110609), **b** T449A (cell C110323), **c** T449Y (cell D110803), and **d** T449V (cell L110331) channels. *Insets* show currents elicited during P3 and are scaled similarly. **e** The fraction of non-inactivated channels (ratio of P3 to P1) is plotted versus inactivating voltage to depict the voltage dependence of inactivation. For T449A, a 1.6 s inactivating pulse was used. WT, T449A, T449Y, and T449V ($n = 5$). T449A is statistically different from WT in the range [−90, 20] mV, and T449Y & T449V in the range [0, 60] mV

Because T449 mutations had very little effect on Shaker activation, their effects on inactivation can be interpreted as effects on the inactivation mechanism itself, not as

Table 1 Kinetics of inactivation

	$\tau_{-20\ mV}$ (s)	$\tau_{+60\ mV}$ (s)
T449A	0.30 ± 0.02	0.22 ± 0.01
ShIR WT	3.93 ± 0.59	1.55 ± 0.09
T449Y	5.27 ± 0.54	3.27 ± 0.21
T449V	5.11 ± 0.54	3.28 ± 0.28

Weighted average time constants from biexponential fits to current traces during channel inactivation (Fig. 2a–d, P2) at the voltages noted. For T449A, time constants are reported for monoexponential fits

secondary effects resulting from modification of the activation process.

Mutation at T449 Reveals Discrete Shaker Inactivation Phenotypes

Fig. 2 depicts the time course of inactivation for WT, T449A, T449Y, and T449V channels at −90, 0, and +60 mV (as labeled), respectively. The kinetics of inactivation during a 10-second inactivating pulse (P2) were described by a biexponential fit except for T449A which used a 1.6-second inactivating pulse and was approximated with a monoexponential fit. T449A channels inactivated most quickly followed by WT, T449V, and T449Y channels (see Table 1). A detailed summary of biexponential fit parameters is presented in Table S3. Fig. S2 juxtaposes inactivation seen in Fig. 2a–d superimposed with exponential fits, and currents during the first 500 ms of the inactivating pulse to better visualize the initial time course of inactivation.

The voltage dependence of inactivation was measured by comparing the amplitude of currents before and after an inactivating pulse. The fraction of non-inactivated channels (P3/P1 ratio) is plotted versus inactivating voltage in Fig. 2e. WT channels inactivated with a monotonic voltage dependence of inactivation, strongest at positive voltages, lacking the U-shaped profile are seen previously (Klemic et al. 2001). T449A channels also exhibited a monotonic voltage dependence of inactivation which was more complete than WT channels throughout the voltage range (except at +60 mV). However, both T449Y and T449V channels inactivated incompletely and had a non-monotonic U-shaped voltage dependence of inactivation different from WT channels at 0, 20, and +60 mV ($p < 0.05$).

The three-pulse protocol of Fig. 2 can only measure the time course of inactivation at voltages which activate a sizable fraction of channels, potentially overlooking the contribution of closed-state inactivation. The three-pulse protocol of Fig. 3 was used to quantify inactivation without the need to first open channels. Figure 3a illustrates this protocol for T449A channels. Fig. 3b–c visualize the time course of inactivation for each mutant at −10 and −40 mV (only −40 mV for T449A). Different subsets of voltages were studied for each mutant (see Fig. S3 for a full summary). Mutants T449Y and T449V were not statistically different from WT channels at −10 or −40 mV (e.g., at −40 mV, inactivation in T449V was 35 ± 4 % complete at 30 s with a time constant of 54.5 ± 7.7 s versus WT 37 ± 9 % complete and 68.2 ± 18.2 s). We suppose that the large variability at −40 mV is due to this voltage being in the steep part of the inactivation curve (Fig. 2e). However, T449A inactivated faster and more completely at −40 mV (89 ± 1 % complete and 2.6 ± 0.7 s). Even at −50 mV, a voltage where only 5.4 ± 1.1 % ($n = 13$) of T449A channels is activated, 46.6 ± 4.5 % ($n = 4$) inactivation could be achieved (Fig. S3b).

To characterize recovery from inactivation, the protocol of Fig. 3 was modified to include a 10-second inactivating pulse to 0 mV after the control pre-pulse. Channels then recover from inactivation (at −90 mV in Fig. 4a for T449Y channels) for a variable duration before measuring the current amplitude during a test pulse. Fig. S4 shows resultant current traces from the protocol of Fig. 4a but with recovery at −140 mV for each of the channels studied.

Recovery was measured for a variety of different voltages (from −140 to −40 mV). The fraction of non-inactivated channels (ratio of post- to pre-pulse) is plotted for WT and mutant channels versus the duration of recovery from inactivation at various voltages in Fig. 3b–e. Recovery from

Table 2 Kinetics of recovery from inactivation

	$\tau_{-140\ mV}$ (s)	$\tau_{-120\ mV}$ (s)	$\tau_{-90\ mV}$ (s)	$\tau_{-60\ mV}$ (s)	$\tau_{-50\ mV}$ (s)
T449A	10.2 ± 1.0	9.02 ± 1.17	10.4 ± 0.3	19.9 ± 3.5	14.7 ± 6.6
ShIR WT	1.23 ± 0.16	1.28 ± 0.16	1.86 ± 0.16	8.46 ± 0.70	9.76 ± 1.49
T449V	0.18 ± 0.02	0.28 ± 0.04	0.86 ± 0.12	4.49 ± 0.96	9.67 ± 0.77
T449Y	0.11 ± 0.01	0.26 ± 0.04	0.82 ± 0.09	4.13 ± 0.70	8.76 ± 1.84

Time constants from monoexponential fits to the time course of recovery from inactivation obtained with the protocol of Fig. 4, at −140 mV ($5 \le n \le 9$), −120 mV ($5 \le n \le 7$), −90 mV ($10 \le n \le 15$), −60 mV ($5 \le n \le 6$), and −50 mV ($5 \le n \le 6$)

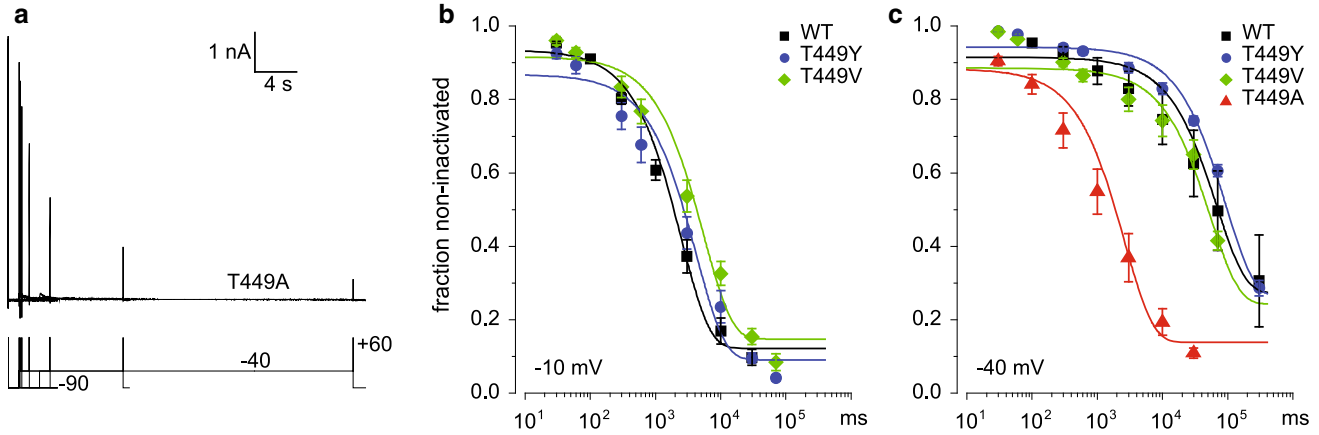

Fig. 3 Inactivation with weak depolarization: **a** 10 ms test pulses to +60 mV measure the amplitude of non-inactivated channels before and after an inactivating pulse to −40 mV of variable duration (from 30 ms to 300 s) for T449A (cell B110302). **b** the fraction of non-inactivated channels (determined by ratio of test pulses in panel a) is plotted versus inactivating time at −10 mV for WT, T449Y, and T449V channels ($n = 5$), and in c at −40 mV for all mutants. WT and T449Y ($n = 5$), T449V ($n = 4$), and T449A ($n = 7$) *Smooth curves* represent monoexponential fits to the time course of inactivation. At −40 mV, T449A is statistically different from WT

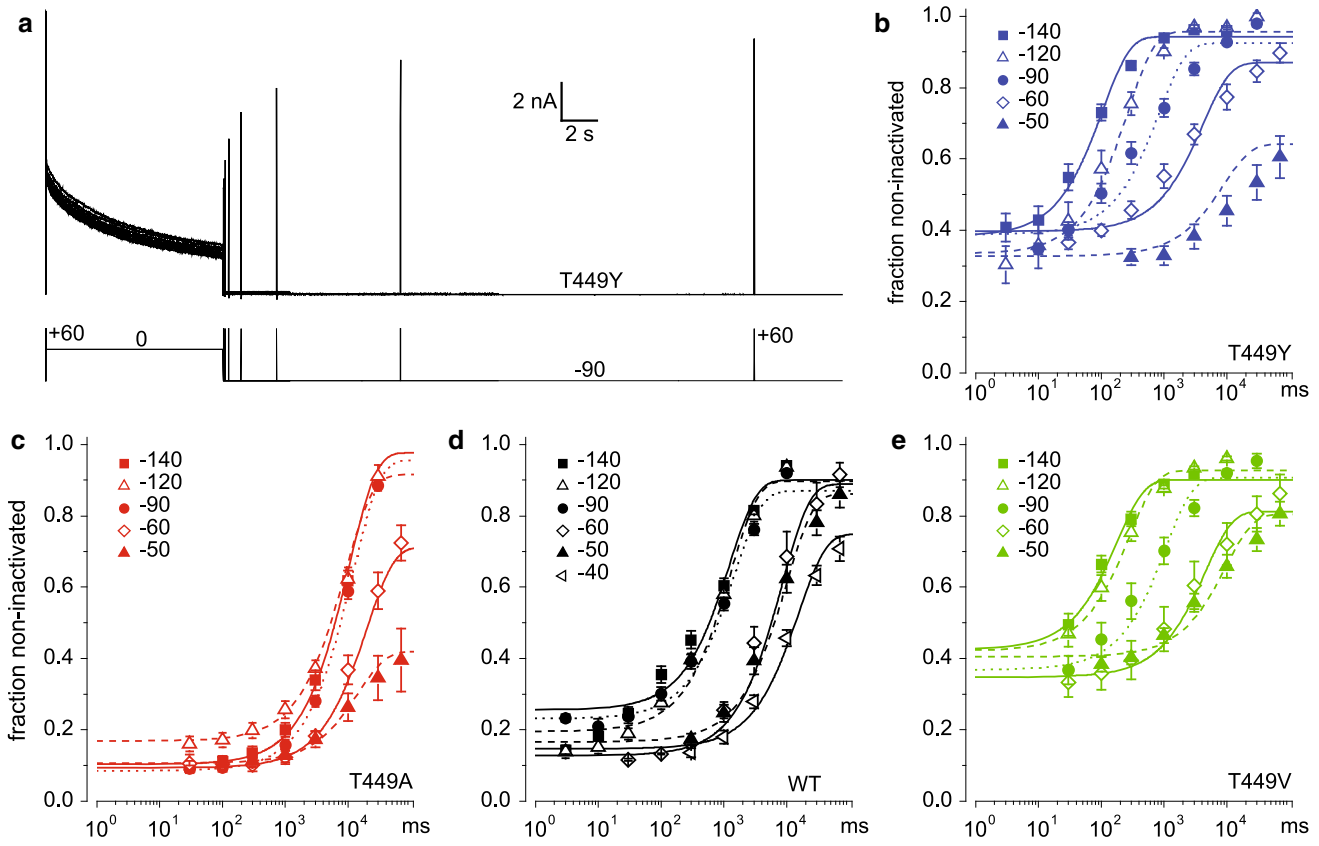

Fig. 4 Recovery from inactivation: **a** 20 ms test pulses to +60 mV measure the amplitude of non-inactivated channels before and after a sequential inactivating pulse to 0 mV for 10 s followed by recovery at −90 mV for a variable duration (from 3 ms to 70 s) for T449Y (cell D110801). **b** the protocol of panel a is repeated at various recovery voltages (from −140 to −40 mV), and the fraction of non-inactivated channels (from the ratio of test pulses in panel a) is plotted versus recovery time for T449Y ($5 \leq n \leq 7$), **c** T449A ($5 \leq n \leq 7$), **d** WT ($5 \leq n \leq 9$), and **e** T449V channels ($5 \leq n \leq 6$). Recovery at −140 mV (*squares*), −120 mV (*open triangles*), −90 mV (*circles*), −60 (*open diamonds*), −50 (*solid triangles*), and −40 (*empty left triangles*). For T449A, a 5 s inactivating pulse was used. *Smooth curves* represent monoexponential fits to the time course of recovery from inactivation

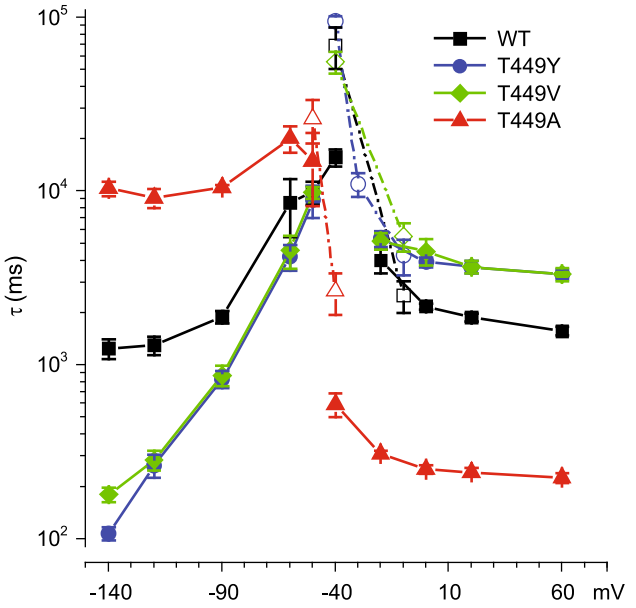

Fig. 5 Kinetics of inactivation and recovery from inactivation: Time constants from monoexponential fits to the time course of recovery from inactivation (Fig. 4b–e) are plotted versus recovery voltage and shown as *solid symbols* from −140 to −40 mV. Time constants from monoexponential fits to the time course of inactivation with weak depolarization (Fig. 3b and c, and Fig. S3b, d, f, and h) are plotted versus inactivating voltage and shown as *open symbols* from −50 to −10 mV. Time constants from monoexponential fits to inactivating currents with strong depolarization (Fig. 2a–d) are plotted versus inactivating voltage and shown as *solid symbols* from −40 to +60 mV. T449A ($4 \leq n \leq 7$), WT ($5 \leq n \leq 9$), T449Y ($5 \leq n \leq 7$), and T449V ($4 \leq n \leq 6$). T449A is statistically different from WT at −140, −120, −90, and the range [−40, +60] mV, and both T449Y & T449V were different from WT at −140, −120, −90, and the range [−20, +60] mV

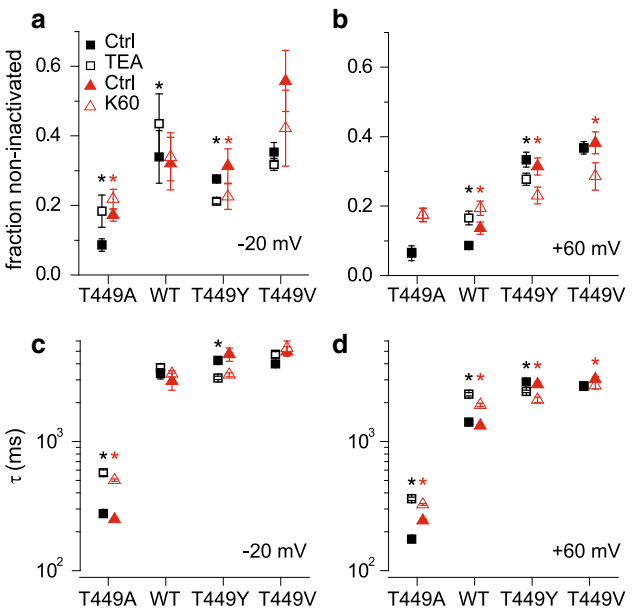

Fig. 6 Extracellular cations' effects on inactivation: The fraction of non-inactivated channels (as calculated in Fig. 2) is plotted for each mutant: control for TEA (*solid squares*), IC_{50} TEA (*empty squares*), control for 60 mM K^+ (*solid triangles*), and 60 mM K^+ (*empty triangles*) at **a** −20 mV and **b** +60 mV. The effect of TEA was statistically different from control in T449A, WT, and T449Y at −20 mV but only WT and T449Y at +60 mV. 60 mM K^+ was statistically different from control in T449A and T449Y at −20 mV and for WT, T449Y, and T449V at +60 mV. Weighted time constants from biexponential fits (WT, T449Y, and T449V) or monoexponential fits (T449A) to inactivating currents were measured (in the presence and absence of added cations) and are plotted for each mutant as above at **c** −20 mV and **d** +60 mV. The effect of TEA was statistically different from control for T449A & T449Y at −20 mV and T449A, WT, & T449Y at +60 mV. The effect of 60 mM K^+ was statistically different from control in T449A at −20 mV, and all channels at +60 mV. T449A ($4 \leq n \leq 5$), WT ($n = 5$), T449Y ($4 \leq n \leq 5$), T449V ($4 \leq n \leq 5$)

inactivation was well characterized by a monoexponential fit for all voltages and mutants (Table 2). For T449A channels, recovery was slow and weakly voltage dependent ($\tau = 10.2 \pm 1.0$ s at −140 mV versus 19.9 ± 3.5 s at −60 mV), whereas recovery was fast and strongly voltage dependent in T449Y and T449V channels (for T449Y: $\tau = 106 \pm 9$ ms at −140 mV versus 4.1 ± 0.7 s at −60 mV). Recovery in WT channels was faster than T449A and more voltage dependent ($\tau = 1.2 \pm 0.2$ s at −140 mV versus 8.5 ± 3.1 s at −60 mV). Fig. S5 is an alternate presentation of Fig. 4, comparing all four mutants at each recovery voltage, providing a direct comparison of the speed of recovery across the mutants.

Figure 5 summarizes the time constants for inactivation and recovery, including monoexponential fits to recovery data (smooth curves, Fig. 4), development of inactivation with weak depolarization (smooth curves, Figs. 3 and S3), and onset of inactivation at strongly depolarized voltages (fits to currents in Fig. 2). This figure demonstrates the slow, weakly voltage-dependent recovery from inactivation in T449A channels combined with fast onset of inactivation at more positive voltages. Furthermore, Fig. 5 highlights the strong voltage dependence of recovery from inactivation in T449Y and T449V channels, yet slower kinetics of inactivation at positive voltages compared to WT.

High Potassium and TEA Affect Shaker T449 Mutants

It is noteworthy that the time course of recovery from inactivation was well approximated by a single exponential process at each voltage, in contrast to the biexponential recovery observed previously for WT channels in Xenopus oocytes (Klemic et al. 2001), where recovery from U-type inactivation was much faster and more voltage dependent than recovery from C-type inactivation. In addition, inactivation was considerably faster in HEK 293 cells than in oocytes (see Discussion). We hypothesized that C-type

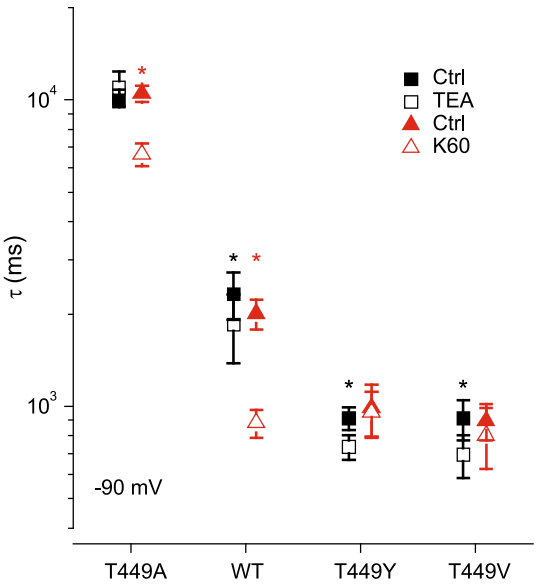

Fig. 7 Extracellular cations' effects on recovery from inactivation: Time constants from monoexponential fits to the time course of recovery from inactivation at −90 mV are plotted for each mutant in the presence and absence of added cations as in Fig. 6. The effect of TEA was statistically different from control in WT, T449Y, and T449V channels. The effect of 60 mM K^+ was statistically different from control in T449A and WT channels. T449A ($4 \leq n \leq 5$), WT ($n = 5$), T449Y ($n = 5$), T449V ($4 \leq n \leq 5$)

inactivation was faster for channels expressed in HEK 293 cells, allowing C-type inactivation to dominate in WT. That is, our working hypothesis was that inactivation was essentially C-type in WT and T449A, but in T449Y and T449V, C-type inactivation was slowed to the extent that the remaining inactivation was essentially all U-type.

Pharmacological methods provide additional criteria for determining how mutants affect C- versus U-type inactivation. Specifically, extracellular application of either 60 mM K^+ or block by TEA was used to evaluate effects on inactivation for each mutant. The effect of both TEA and elevated K^+ was tested with the three-pulse protocol of Fig. 2 (development of inactivation, Fig. 6) and four-pulse protocol of Fig. 4 (recovery from inactivation at −90 mV, Fig. 7). Recordings in TEA or elevated K^+ were compared to control recordings (the average of values recorded before application and after washout).

For WT channels, TEA at the IC_{50} concentration significantly decreased the amount of inactivation at −20 mV (Fig. 6a), but had no effect on the speed of inactivation at −20 mV (Fig. 6c), whereas the effect of both TEA and 60 mM K^+ was significant for both phenomena at +60 mV (Fig. 6b and d).

For T449A channels, both TEA and K^+ significantly decreased the extent of inactivation at −20 mV (Fig. 6a) and had no effect at +60 mV, possibly since inactivation here is nearly complete. TEA and K^+ significantly slowed the kinetics of inactivation at both −20 and +60 mV (Fig. 6c and d). In contrast, in T449Y channels, both TEA and K^+ enhanced the extent of inactivation at both −20 and +60 mV (Fig. 6a and b); moreover, the rate of inactivation was increased in TEA at −20 mV and both TEA and K^+ at +60 mV. In T449V channels, only elevated K^+ significantly enhanced and sped inactivation at +60 mV.

Lastly, the effects of extracellular K^+ or TEA on kinetics of recovery from inactivation at −90 mV were evaluated (Fig. 7). Elevated extracellular potassium significantly hastened recovery from inactivation in both WT and T449A channels. However, TEA significantly sped recovery in WT, T449Y, and T449V channels.

Modeling Supports Existence of Two Inactivation Phenotypes

A 12-state allosteric model describing inactivation of $K_V2.1$ channels (Klemic et al. 1998) was used to describe Shaker IR mutants and understand their preference for open- versus closed-state inactivation (Fig. S6a). Using the Q-Matrix method (Colquhoun and Hawkes 1995) to simulate macroscopic currents, the model was adapted in MATLAB to permit automated estimation of the model's 11 parameters (Jamieson and Jones 2013). Parameters were estimated for two datasets per mutant, including WT channels, for a total of eight datasets (see supplementary material).

We hypothesized that each mutant possessed one predominant inactivation mechanism. Therefore, we first attempted fitting currents to a 12-state model with one set of connected closed-inactivated and open-inactivated states (Fig. S6a). That scheme could satisfactorily describe key features of WT and mutant channel data without requiring two independent inactivation pathways, e.g., an 18-state model allowing C- and U-type inactivation to occur independently (Klemic et al. 2001). The model replicated the monotonic voltage dependence of inactivation for T449A and WT channels (Fig. 8a), while reproducing the U-shaped voltage dependence of T449Y and T449V channels (Fig. 8b). Furthermore, the model was able to describe the weak voltage dependence of recovery from inactivation of T449A channels and the intermediate voltage dependence of WT channels (Fig. 8c), while simulating the strong voltage dependence of recovery from inactivation for T449Y/V mutants (Fig. 8d). Notably, the model was able to reproduce the fast inactivation kinetics of T449A channels (Fig. 8c), the intermediate kinetics of WT channels (Fig. 8c), and the slow kinetics of T449Y/V channels (Fig. 8d). The extent of inactivation was modeled accurately for all datasets, except that too much inactivation was predicted for most datasets near −40 mV, where

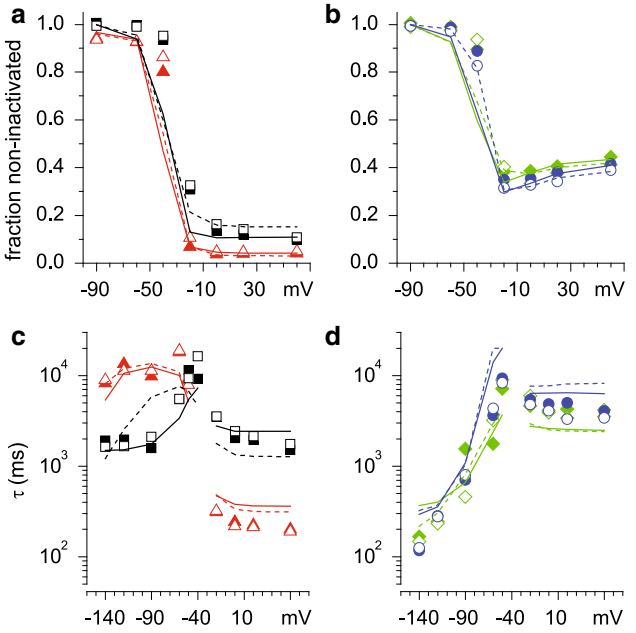

Fig. 8 Model simulations of voltage dependence of inactivation and recovery: The protocol of Fig. 2 is simulated with the 12-state model, depicting the fraction of non-inactivated channels. Data are depicted as symbols with fitted model depicted as curves as follows: **a** WT dataset T1 (*solid curve fitting solid squares*), WT dataset T2 (*dashed curve fitting open squares*), T449A dataset A1 (*solid curve fitting solid triangles*), and T449A dataset A2 (*dashed curve fitting open triangles*) **b** T449Y dataset Y1 (*solid curve fitting solid circles*), T449Y dataset Y2 (dashed curve fitting open circles), T449V dataset V1 (*solid curve fitting solid diamonds*), and T449V dataset V2 (*dashed curve fitting open diamonds*). The kinetics of recovery of inactivation and onset of inactivation as in Fig. 5 are shown as simulated by the model for **c** WT and T449A, and **d** T449Y and T449V: *symbols and curves* as a and b

both activation and inactivation were steeply voltage dependent. The time course of inactivation was described less well, as discussed in the Supplementary Material. In particular, despite the multiple inactivated states, the time course of inactivation predicted by the model was essentially monoexponential, although inactivation was incomplete (as observed experimentally).

Although the model was able to reproduce many qualitative and quantitative features of the data, some model parameters were variable even between different datasets from the same mutant, as we found previously for our study on $K_V2.1$ (Jamieson and Jones 2013). Despite the variability in parameter values, the resulting models can yield quantitatively similar model behavior; this is explored in the Supplementary Material. However, some parameters remain informative, notably the allosteric parameter "g" controlling the rate of inactivation from the open state relative to the nearest closed state, see Table S4. Relative to WT channels, "g" was much larger for the T449A mutant (g >30) but smaller for the T449Y/V mutants (g <0.3), suggesting two fundamentally different inactivation phenotypes, with preferential open-state inactivation for T449A but preferential closed-state inactivation for T449Y/V.

Discussion

Mutations at T449 in Shaker IR can either speed or slow inactivation, leading to rates varying over 3 orders of magnitude (López-Barneo et al. 1993). This was initially interpreted in terms of a single (C-type) inactivation process, but Shaker IR also exhibits U-type inactivation (Klemic et al. 2001). This study examines which form of inactivation is affected by mutation. We conclude that C-type inactivation is selectively affected, with no clear effect on U-type inactivation, in agreement with our previous study on U-type inactivation of $K_V2.1$ (Jamieson and Jones 2013).

Activation

Shaker channels activate with steep voltage dependence (Figs. 1c and S1). If inactivation obtains most or all of its voltage dependence from coupling to the activation process (Armstrong and Bezanilla 1977), as we assume in our kinetic model, this means that careful analysis of potential effects of mutations on activation must be considered before concluding that there are direct effects on the inactivation mechanism. A previous study of T449 mutants reported no significant changes in activation kinetics for T449A, T449Y, or T449V, but quantitative data supporting this observation were not shown in detail (López-Barneo et al. 1993). The significantly slower activation kinetics we observed at some voltages in T449Y and T449V channels are a novel observation. If inactivation in these mutants occurs only after channels open, we would expect at most 1.3- to 2-fold slower inactivation kinetics.

Activation of Shaker IR channels has been comprehensively studied previously in Xenopus oocytes (Zagotta et al. 1994a; Schoppa and Sigworth 1998b; Zagotta et al. 1989). Therefore, the main reason for presenting data on activation kinetics in this study is as a control for mutations at Shaker T449 expressed in HEK cells in whole-cell configuration. This data also serve as a basis for constraining activation kinetics in our kinetic model, which uses a linear scheme where voltage sensor activation is followed by channel opening (Zagotta and Aldrich 1990), rather than the more complex models proposed subsequently.

Our data on activation of Shaker IR are generally consistent with previous studies, with some quantitative differences. Time constants for activation were ~2-fold

slower than reported for outside-out patches from Xenopus oocytes (Zagotta et al. 1994b; Schoppa and Sigworth 1998a). The midpoint of the activation curve was 13 mV more positive than a previous study (Zagotta et al. 1994b), with both fitted to a 4th power Boltzmann, and 7 mV more positive than a more recent study (Phillips and Swartz 2010), fitted to a Boltzmann with z = 3.3.

Inactivation of WT Shaker IR

Inactivation was 6-fold faster in our whole-cell recordings from HEK cells than in our previous study in Xenopus oocytes (Klemic et al. 2001). This is reminiscent of previous studies finding relatively rapid inactivation ($\tau \sim 1$ s) in either inside-out or outside-out patches from Xenopus oocytes (Hoshi et al. 1991; López-Barneo et al. 1993; Oliva et al. 2005) or HEK cells (Yellen et al. 1994) but slower inactivation ($\tau = 4$–8 s) in two electrode or cut-open recordings from whole oocytes (Olcese et al. 1997; Klemic et al. 2001; Oliva et al. 2005; Gonzalez-Perez et al. 2008). It is not clear why the rate of inactivation depends on the expression system, but this observation is consistent with previous evidence that slow inactivation of Shaker IR can be modulated, e.g., by methionine oxidation (Chen et al. 2000).

We previously concluded that slow inactivation of Shaker IR in Xenopus oocytes was approximately half C-type and half U-type (Klemic et al. 2001). Which process is different in our study on HEK cells? Several lines of evidence suggest that C-type inactivation dominates. First, there is no U-shape to the inactivation curve (Fig. 2e), contrasting with the expectation for U-type inactivation (Klemic et al. 1998; Klemic et al. 2001; Jamieson and Jones 2013). Second, recovery from inactivation is slow and weakly voltage dependent (Figs. 4 and 5), similar to the slow component previously interpreted as recovery from C-type inactivation (Klemic et al. 2001). Finally, inactivation was slowed by external TEA or high K^+_o, as expected for C,- but not U-type inactivation (Fig. 6). We conclude that C-type inactivation of Shaker IR is significantly faster in HEK cells than in whole-oocyte recordings from Xenopus, similar to a previous explanation of the difference between patch and whole-cell recordings from oocytes (Oliva et al. 2005). This can explain the effective absence of U-type inactivation, since channels that inactivate by a C-type mechanism are effectively protected from U-type inactivation.

At most voltages, recovery from inactivation of WT channels was well approximated by a single exponential, consistent with a single inactivation process. A hint of a fast component was visible at the most negative voltages tested (Fig. S5), where the difference in recovery rates between C- and U-type inactivation is maximal (Klemic et al. 2001) (see also Fig. 5 here). This may indicate a small amount of U-type inactivation. However, our model, which includes a single inactivation process for each mutant, did provide an adequate description of inactivation and recovery in WT channels, suggesting that any contribution of U-type inactivation is negligible.

For the best parameter sets found, most inactivation in WT channels occurs directly from the open state. This is primarily because the C–O transition is strongly forward biased, so channels spend little time in partially activated closed states. That forward bias was found for all mutations, and differs from $K_V2.1$ (Klemic et al. 1998; Jamieson and Jones 2013). At the microscopic level, open- and closed-state inactivation occur at comparable rates from C4 and from O ($g = 0.4$ and 1.2 for the two datasets fitted). The models also suggest that recovery though closed-inactivated states is necessary to explain the mild voltage dependence observed for recovery. This not only supports the common idea that C-type inactivation is predominantly open-state inactivation, but also supports a role for closed-inactivated states even in C-type inactivation.

Inactivation in Shaker IR T449A

This mutation dramatically sped inactivation in agreement with previous observations (López-Barneo et al. 1993; Meyer and Heinemann 1997; Panyi and Deutsch 2006), while slowing recovery (Figs. 2–5). Modeling suggests that these effects result from direct effects on both the microscopic inactivation and recovery processes. Inactivation in T449A is clearly C-type, given the absence of a U-shaped inactivation curve (Fig. 2e), the slow and nearly voltage-independent recovery from inactivation (Figs. 4 and 5), and sensitivity to external TEA and high K^+_o (Fig. 6). Indeed, our modeling suggests that inactivation and recovery can be quantitatively described by pure open-state inactivation (Fig. S6b), where inactivation occurs only from the open state. Simulated recovery through the open state is very slow, but still sufficiently rapid to explain the very slow recovery from inactivation observed experimentally. We cannot completely exclude closed-inactivated states for T449A, in part, since some simulations produced slightly lower total error with a pathway where recovery did involve the I4 state (see Supplementary Material).

Inactivation in Shaker IR T449V and T449Y

These mutants slightly slowed the rate of inactivation (Fig. 2). The effect was less severe than originally reported (López-Barneo et al. 1993), but consistent with more recent studies (Holmgren et al. 1996; Peters et al. 2011). Quantitatively slower inactivation is expected if these mutations

slow, or eliminate, C-type inactivation, revealing U-type inactivation. Similar effects have been reported for certain mammalian K_V1 channels, specifically slow-inactivating mutants $K_V1.3$ H404V (Nguyen et al. 1996), $K_V1.4$ K532Y (Rasmusson et al. 1995), and K532V (Oliver et al. 2004), as well as $K_V1.5$ analogs R487Y (Fedida et al. 1999) and R487V (Fedida et al. 1999; Zhang et al. 2003).

Recovery from inactivation was fast and voltage dependent, as expected for U-type inactivation. In contrast to the other constructs examined and to expectations for C-type inactivation, TEA and high K^+_o actually sped inactivation, as previously reported for U-type inactivation (Klemic et al. 1998, 2001; Jamieson and Jones 2013). We conclude that these mutations reveal a pre-existing U-type inactivation pathway in Shaker IR, which is bypassed in WT channels given the relatively fast C-type inactivation.

Our model reproduced the combination of slow inactivation and fast voltage-dependent inactivation for these two mutants. Notably, the factor "g" was less than 0.3 for all 4 datasets, indicating preferential closed-state inactivation, and comparable to our values for U-type inactivation of $K_V2.1$ (Jamieson and Jones 2013). Correspondingly, at negative voltages, closed-state inactivation dominated. For example, at −40 mV for T449V dataset V1, 35 % of channels were in closed-inactivated states versus 9 % in the open-inactivated state at steady state. However, the strongly forward-biased C–O step allowed most channels to accumulate in the open-inactivated state at strongly depolarized voltages. This supports the idea that U-type inactivation occurs preferentially, but not at all exclusively, from closed states.

Conclusions

We conclude that WT Shaker IR channels inactivate predominantly via a C-type mechanism (when expressed in HEK cells). T449A speeds C-type inactivation, whereas the T449Y and T449V mutations slow it to the extent that predominant U-type inactivation is revealed. Thus, mutations of T449 can be interpreted as affecting C-type inactivation exclusively, sparing U-type. Mutations at the corresponding site can be added to the array of tools for distinguishing C- from U-type inactivation in other potassium channels. We also argue that C- and U-type inactivation, respectively, target open and closed states preferentially, but not exclusively. If each mechanism involves both open-inactivated and closed-inactivated states, it is not correct to identify C-type inactivation with open-state inactivation or U-type inactivation with closed-state inactivation.

Acknowledgments This work was supported, in part, by the National Institutes of Health grant NS24771 to S.W. Jones. We thank the CWRU ITS High Performance Computing Cluster for computational time. We also thank Dr. Gary Yellen for the gift of the GW1-CMV expression vector containing the Shaker IR T449V channel.

References

Armstrong CM, Bezanilla F (1977) Inactivation of the sodium channel. II. Gating current experiments. J Gen Physiol 70(5):567–590

Barghaan J, Bähring R (2009) Dynamic coupling of voltage sensor and gate involved in closed-state inactivation of Kv4.2 channels. J Gen Physiol 133(2):205–224

Baukrowitz T, Yellen G (1996) Use-dependent blockers and exit rate of the last ion from the multi-ion pore of a K^+ channel. Science 271(5249):653–656

Carrillo E, Arias O II, Islas LD, Gomez-Lagunas F (2013) Shab K^+ channel slow inactivation: a test for U-type inactivation and a hypothesis regarding K^+-facilitated inactivation mechanisms. Channels 7(2):97–108

Chen JG, Avdonin V, Ciorba MA, Heinemann SH, Hoshi T (2000) Acceleration of P/C-type inactivation in voltage-gated K^+ channels by methionine oxidation. Biophys J 78(1):174–187

Cheng YM, Azer J, Niven CM, Mafi P, Allard CR, Qi J, Thouta S, Claydon TW (2011) Molecular determinants of U-type inactivation in Kv2.1 channels. Biophys J 101(3):651–661

Choi KL, Aldrich RW, Yellen G (1991) Tetraethylammonium blockade distinguishes two inactivation mechanisms in voltage-activated K^+ channels. Proc Natl Acad Sci USA 88(12):5092–5095

Colquhoun D, Hawkes AG (1995) A Q-matrix cookbook. How to write only one program to calculate the single-channel and macroscopic predictions for any kinetic mechanism. In: Sakmann B, Neher E (eds) Single-Channel Recording, 2nd edn. Plenum Press, New York

Cordero-Morales JF, Cuello LG, Zhao Y, Jogini V, Cortes DM, Roux B, Perozo E (2006) Molecular determinants of gating at the potassium-channel selectivity filter. Nat Struct Mol Biol 13:311–318

Cordero-Morales JF, Jogini V, Lewis A, Vasquez V, Cortes DM, Roux B, Perozo E (2007) Molecular driving forces determining potassium channel slow inactivation. Nat Struct Mol Biol 14:1062–1069

Cuello LG, Jogini V, Cortes DM, Perozo E (2010) Structural mechanism of C-type inactivation in K^+ channels. Nature 466(7303):203–208

Dougherty K, De Santiago-Castillo JA, Covarrubias M (2008) Gating charge immobilization in Kv4.2 channels: the basis of closed-state inactivation. J Gen Physiol 131(3):257–273

Fedida D, Maruoka ND, Lin SP (1999) Modulation of slow inactivation in human cardiac Kv1.5 channels by extra- and intracellular permeant cations. J Physiol (Lond) 515(2):315–329

Frazier CJ, George EG, Jones SW (2000) Apparent change in ion selectivity caused by changes in intracellular K^+ during whole-cell recording. Biophys J 78(4):1872–1880

Gonzalez-Perez V, Neely A, Tapia C, Gonzalez-Gutierrez G, Contreras G, Orio P, Lagos V, Rojas G, Estevez T, Stack K, Naranjo D (2008) Slow inactivation in Shaker K channels is delayed by intracellular tetraethylammonium. J Gen Physiol 132(6):633–650

Holmgren M, Jurman ME, Yellen G (1996) N-type inactivation and the S4-S5 region of the Shaker K^+ channel. J Gen Physiol 108(3):195–206

Hoshi T, Zagotta WN, Aldrich RW (1991) Two types of inactivation in Shaker K^+ channels: effects of alterations in the carboxy-terminal region. Neuron 7(4):547–556

Jamieson Q, Jones SW (2013) Role of outer-pore residue Y380 in U-type inactivation of Kv2.1 channels. J Membr Biol 246(8):633–645

Kerschensteiner D, Monje F, Stocker M (2003) Structural determinants of the regulation of the voltage-gated potassium channel Kv2.1 by the modulatory α-subunit Kv9.3. J Biol Chem 278:18154–18161

Klemic KG, Shieh C–C, Kirsch GE, Jones SW (1998) Inactivation of Kv2.1 potassium channels. Biophys J 74(4):1779–1789

Klemic KG, Kirsch GE, Jones SW (2001) U-type inactivation of Kv3.1 and Shaker potassium channels. Biophys J 81(2):814–826

Liu Y, Jurman ME, Yellen G (1996) Dynamic rearrangement of the outer mouth of a K^+ channel during gating. Neuron 16(4):859–867

López-Barneo J, Hoshi T, Heinemann SH, Aldrich RW (1993) Effects of external cations and mutations in the pore region on C-type inactivation of Shaker potassium channels. Receptors Channels 1(1):61–71

Meyer R, Heinemann SH (1997) Temperature and pressure dependence of Shaker K^+ channel N- and C-type inactivation. Eur Biophys J 26(6):433–445

Nguyen A, Kath JC, Hanson DC, Biggers MS, Canniff PC, Donovan CB, Mather RJ, Bruns MJ, Rauer H, Aiyar J, Lepple-Wienhues A, Gutman GA, Grissmer S, Cahalan MD, Chandy KG (1996) Novel nonpeptide agents potently block the C-type inactivated conformation of Kv1.3 and suppress T cell activation. Mol Pharmacol 50(6):1672–1679

Ogielska EM, Zagotta WN, Hoshi T, Heinemann SH, Haab J, Aldrich RW (1995) Cooperative subunit interactions in C-type inactivation of K channels. Biophys J 69(6):2449–2457

Olcese R, Latorre R, Toro L, Bezanilla F, Stefani E (1997) Correlation between charge movement and ionic current during slow inactivation in Shaker K^+ channels. J Gen Physiol 110(5):579–589

Oliva C, Gonzalez VM, Naranjo D (2005) Slow inactivation in voltage gated potassium channels is insensitive to the binding of pore occluding peptide toxins. Biophys J 27:27

Oliver D, Lien CC, Soom M, Baukrowitz T, Jonas P, Fakler B (2004) Functional conversion between A-type and delayed rectifier K^+ channels by membrane lipids. Science 304(5668):265–270

Panyi G, Deutsch C (2006) Cross talk between activation and slow inactivation gates of Shaker potassium channels. J Gen Physiol 128(5):547–559

Peters CJ, Werry D, Gill HS, Accili EA, Fedida D (2011) Mechanism of accelerated current decay caused by an episodic ataxia type-1-associated mutant in a potassium channel pore. J Neurosci 31(48):17449–17459

Phillips LR, Swartz KJ (2010) Position and motions of the S4 helix during opening of the Shaker potassium channel. J Gen Physiol 136(6):629–644

Rasmusson RL, Morales MJ, Castellino RC, Zhang Y, Campbell DL, Strauss HC (1995) C-type inactivation controls recovery in a fast inactivating cardiac K^+ channel (Kv1.4) expressed in Xenopus oocytes. J Physiol (Lond) 489 (3):709-721

Schoppa NE, Sigworth FJ (1998a) Activation of Shaker potassium channels I. Characterization of voltage-dependent transitions. J Gen Physiol 111(2):271–294

Schoppa NE, Sigworth FJ (1998b) Activation of Shaker potassium channels III. An activation gating model for wild-type and V2 mutant channels. J Gen Physiol 111(2):313–342

Trapani JG, Korn SJ (2003) Control of ion channel expression for patch clamp recordings using an inducible expression system in mammalian cell lines. BMC Neurosci 4:15

Yellen G, Sodickson D, Chen TY, Jurman ME (1994) An engineered cysteine in the external mouth of a K^+ channel allows inactivation to be modulated by metal binding. Biophys J 66(4):1068–1075

Zagotta WN, Aldrich RW (1990) Voltage-dependent gating of Shaker A-type potassium channels in Drosophila muscle. J Gen Physiol 95(1):29–60

Zagotta WN, Hoshi T, Aldrich RW (1989) Gating of single Shaker potassium channels in Drosophila muscle and in Xenopus oocytes injected with Shaker mRNA. Proc Natl Acad Sci USA 86(18):7243–7247

Zagotta WN, Hoshi T, Aldrich RW (1994a) Shaker potassium channel gating. III: evaluation of kinetic models for activation. J Gen Physiol 103(2):321–362

Zagotta WN, Hoshi T, Dittman J, Aldrich RW (1994b) Shaker potassium channel gating. II: transitions in the activation pathway. J Gen Physiol 103(2):279–319

Zhang S, Kurata HT, Kehl SJ, Fedida D (2003) Rapid induction of P/C-type inactivation is the mechanism for acid-induced K^+ current inhibition. J Gen Physiol 121(3):215–225